Published in IET Power Electronics
Received on 25th September 2013
Revised on 8th January 2014
Accepted on 1st February 2014
doi: 10.1049/iet-pel.2013.0740

ISSN 1755-4535

Two simple overmodulation algorithms for space vector modulated three-phase to three-phase matrix converter

Amir Masoud Bozorgi, Mohammad Monfared, Habib Rajabi Mashhadi

Department of Electrical Engineering, Ferdowsi University of Mashhad, Mashhad, Iran
E-mail: amir.bozorgi@ieee.org

Abstract: In this study, the potential of the space vector modulation (SVM) to control the matrix converter beyond its intrinsic voltage transfer ratio (VTR) limitation (0.866) is investigated. Afterwards, a simple space vector overmodulation method to increase the VTR of matrix converter is proposed. Depending on the desired VTR, the method is divided into two modes. In the first mode, besides improving the VTR, the quality of the reference quantities is of main concern. In the second mode, the main goal is to reach the maximum achievable VTR at the expense of increased harmonic ripples in the converter waveforms. It is demonstrated that the maximum achievable VTR in both modes depends on the ratio of the desired output frequency to the input frequency. Experimental results confirm the feasibility and appropriate performance of the proposed method.

1 Introduction

The growing demand for AC–AC electric power conversion in industrial applications, and serious attempts to reduce the total cost and size of converters led to the emergence and development of the matrix converter. A matrix converter is made up of an array of bidirectional power semiconductor switches, which directly connect the power supply to the load. The lack of DC-link capacitors in the matrix converter results in increased longevity and reliability in comparison with the conventional back-to-back pulse-width modulated (PWM) converters. Furthermore, the bidirectional power flow capability, sinusoidal input/output waveforms, the ability to control both the amplitude and frequency of output voltage as well as adjustable input power factor have suited it to many industrial applications [1].

Several modulation strategies for the matrix converter have been reported [1–4]. As the first major work on the modulation of the matrix converter, Alesina and Venturini [5] established a PWM algorithm based on a rigorous mathematical approach. The possibility of controlling the output voltage, the ability to adjust the input power factor (on condition that the output power factor is known) and the maximum voltage transfer ratio (VTR) of 0.5 are the main characteristics of this approach. They later proposed injecting the third harmonic of the input and output voltage waveforms into the target outputs in order to increase the VTR from 0.5 to $\sqrt{3}/2 \simeq 0.866$ [6]. They proved that independent of the adopted modulation strategy, the maximum achievable VTR for the matrix converter under linear operation is 0.866. Huber and Borojevic proposed a different waveform synthesis approach based on the space vector modulation (SVM) technique [7, 8]. Sinusoidal waveforms, the ability to control the input power factor, independence of the output power factor and the possibility of achieving the maximum VTR (0.866) are the most significant features of this modulation technique.

The limited maximum achievable VTR is always considered a serious disadvantage in many applications, such as the induction motor drive, where the maximum available magnitude of the output voltage should be equal or a little bit less than the magnitude of the input voltage. In the case of the variable speed drive system for an induction motor, reduction in the output voltage, in addition to the deteriorated dynamic performance, leads to the reduction of the available torque.

To improve the VTR of the matrix converter, several works have been carried out [9–14]. Several studies have introduced different topologies [10] leading to VTRs > 1 at the expense of higher complexity and losses because of additional switches and the existence of passive components.

Another method to increase the VTR of the conventional matrix converter without using extra components is to work in overmodulation region [11–14]. In [12], the matrix converter is divided into a fictitious rectifier and a fictitious inverter stage and the so-called indirect modulation technique was proposed. The indirect technique with a fictitious DC-link adopts the available well-known modulation techniques to the matrix converters. The higher VTR up to 1.053 is achieved at the expense of very high-amplitude low-frequency distortions in the input and output waveforms. Some other modulation methods have presented the overmodulation strategies for their approaches [13, 14]. Complexity, significant low-order harmonics in output quantities and failure to use the real potential of the matrix converter to achieve higher VTRs are the

disadvantages of these methods. There are no papers about extending the operation of the direct SVM technique to the overmodulation region as far as authors know. In this paper, the authors investigated the potential of the SVM to control the matrix converter beyond its intrinsic VTR limitation of 0.866. Then, considering the final goal of this study, which is to increase the VTR of the three-phase to three-phase matrix converter, a space vector overmodulation technique is proposed for the first time.

With regard to similarities between the SVM for matrix converters and the SVM for voltage source inverters (VSIs), in this paper, the already available overmodulation technique for VSIs is adopted in an attempt to boost the VTR of the SVM-controlled matrix converter. Simplicity, extracting the maximum benefit out of the available capacity to achieve the higher VTR and a rather low total harmonic distortion (THD) in the synthesised waveforms are the main features of the proposed overmodulation method. The rest of the paper is organised as follows. In Section 2, after presenting the matrix converter fundamentals, the direct SVM for the matrix converter is formulated. In the next section, the existing capacity of the SVM to increase the VTR of the matrix converter is demonstrated. After explaining the fundamental difference between the VSI and the matrix converter space vector overmodulation, a novel overmodulation method is proposed. Experimental results are presented to support the theoretical achievements. Section 6 concludes the paper.

2 Matrix converter SVM

A matrix converter consists of $m \times n$ bidirectional switches connecting m input phases to n output phases. Usually, voltage sources exist in the input side, and in the output side, there is an induction motor (R–L load) which can be modelled by current sources. Fig. 1 depicts a three-phase to three-phase matrix converter.

According to the Kirchhoff's voltage and current laws, the output and input quantities can be related to each other as follows

$$\begin{pmatrix} v_{an}(t) \\ v_{bn}(t) \\ v_{cn}(t) \end{pmatrix} = \begin{pmatrix} S_{Aa} & S_{Ba} & S_{Ca} \\ S_{Ab} & S_{Bb} & S_{Cb} \\ S_{Ac} & S_{Bc} & S_{Cc} \end{pmatrix} \begin{pmatrix} v_{AN}(t) \\ v_{BN}(t) \\ v_{CN}(t) \end{pmatrix} \quad (1)$$

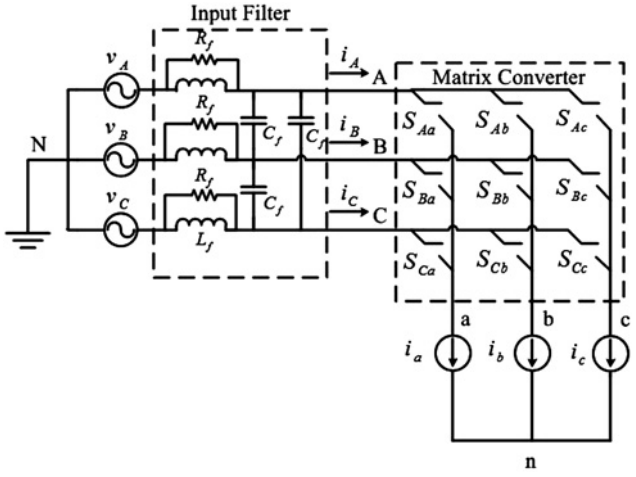

Fig. 1 *Structure of a three-phase to three-phase matrix converter*

$$\begin{pmatrix} i_{AN}(t) \\ i_{BN}(t) \\ i_{CN}(t) \end{pmatrix} = \begin{pmatrix} S_{Aa} & S_{Ba} & S_{Ca} \\ S_{Ab} & S_{Bb} & S_{Cb} \\ S_{Ac} & S_{Bc} & S_{Cc} \end{pmatrix}^T \begin{pmatrix} i_{an}(t) \\ i_{bn}(t) \\ i_{cn}(t) \end{pmatrix} \quad (2)$$

in which the switching function is defined as

$$S_{ij}(t) = \begin{cases} 1, & \text{if switch ON} \\ 0, & \text{if switch OFF} \end{cases}, \quad i \in \{A, B, C\}, j \in \{a, b, c\} \quad (3)$$

On the other hand, to avoid shorting the source voltages and interrupting the load currents, the following constraints must be satisfied

$$\sum_i S_{ij}(t) = 1, \quad i \in \{A, B, C\}, \forall j \in \{a, b, c\} \quad (4)$$

2.1 Direct SVM

The SVM is one of the most common modulation techniques for the matrix converter. This modulation is based on transforming the input and output quantities into the space vectors. The space vector of three-phase quantities can be obtained through the following transformation

$$\bar{X} = \frac{2}{3}\left(x_a + \bar{a}x_b + \bar{a}^2 x_c\right) \quad (5)$$

where x_a, x_b and x_c are the three-phase quantities, and $\bar{a}$ is a complex constant defined as

$$\bar{a} = e^{j(2\pi/3)} = \cos\left(\frac{2\pi}{3}\right) + j\sin\left(\frac{2\pi}{3}\right) \quad (6)$$

Therefore the output voltage and input current vectors can be expressed as

$$\bar{V}_{out} = \frac{2}{3}\left(v_a + v_b e^{j(2\pi/3)} + v_c e^{j(4\pi/3)}\right) = V_{om} e^{j\omega_o t - \varphi_o} \quad (7)$$

$$\bar{I}_{in} = \frac{2}{3}\left(i_A + i_B e^{j(2\pi/3)} + i_C e^{j(4\pi/3)}\right) = I_{im} e^{j\omega_i t - \varphi_i} \quad (8)$$

where ω_o and ω_i are the output and input angular frequencies, respectively, and φ_o and φ_i are the initial angles of the output voltage and input current vectors, respectively. Furthermore, the amplitude of the output voltage and input current are indicated with V_{om} and I_{im}, respectively.

Now, among 27 different possible states, imposed by (4), only 21 states leading to stationary vectors are used for the SVM. Substituting their corresponding output voltages and input currents in (7) and (8), respectively, Table 1 is derived.

The first 18 vectors have fixed directions with magnitudes that vary with the amplitude of input voltage and output current. Fig. 2 depicts these active vectors.

To better clarify the SVM idea, consider $\bar{V}_{out}$ and $\bar{I}_{in}$ to be in sectors 1 and 3, respectively, as represented in Fig. 2. The reference vectors can be synthesised by resolving them into the adjacent active space vectors. Given that both output voltage and input current vectors should be synthesised simultaneously, only the vectors that contribute to both output voltage and input current waveforms shaping must be selected. As a result and in this example, among the adjacent active states, only (±1, ±2, ±7, ±8) switching

doi: 10.1049/iet-pel.2013.0740

Table 1 Possible switching states and relevant space vectors

On switches			States	$\lvert\bar{\boldsymbol{v}}_o\rvert$	$\angle\bar{\boldsymbol{v}}_o$	$\lvert\bar{\boldsymbol{i}}_{in}\rvert$	$\angle\bar{\boldsymbol{i}}_{in}$
S_{Aa}	S_{Bb}	S_{Bc}	+1	$2/3v_{AB}$	0	$2/\sqrt{3}i_a$	$-\pi/6$
S_{Ba}	S_{Ab}	S_{Ac}	−1	$-2/3v_{AB}$	0	$-2/\sqrt{3}i_a$	$-\pi/6$
S_{Ba}	S_{Cb}	S_{Cc}	+2	$2/3v_{BC}$	0	$2/\sqrt{3}i_a$	$\pi/2$
S_{Ca}	S_{Bb}	S_{Bc}	−2	$-2/3v_{BC}$	0	$-2/\sqrt{3}i_a$	$\pi/2$
S_{Ca}	S_{Ab}	S_{Ac}	+3	$2/3v_{CA}$	0	$2/\sqrt{3}i_a$	$7\pi/6$
S_{Aa}	S_{Cb}	S_{Cc}	−3	$-2/3v_{CA}$	0	$-2/\sqrt{3}i_a$	$7\pi/6$
S_{Ba}	S_{Ab}	S_{Bc}	+4	$2/3v_{AB}$	$2\pi/3$	$2/\sqrt{3}i_b$	$-\pi/6$
S_{Aa}	S_{Bb}	S_{Ac}	−4	$-2/3v_{AB}$	$2\pi/3$	$-2/\sqrt{3}i_b$	$-\pi/6$
S_{Ca}	S_{Bb}	S_{Cc}	+5	$2/3v_{BC}$	$2\pi/3$	$2/\sqrt{3}i_b$	$\pi/2$
S_{Ba}	S_{Cb}	S_{Bc}	−5	$-2/3v_{BC}$	$2\pi/3$	$-2/\sqrt{3}i_b$	$\pi/2$
S_{Aa}	S_{Cb}	S_{Ac}	+6	$2/3v_{CA}$	$2\pi/3$	$2/\sqrt{3}i_b$	$7\pi/6$
S_{Ca}	S_{Ab}	S_{Cc}	−6	$-2/3v_{CA}$	$2\pi/3$	$-2/\sqrt{3}i_b$	$7\pi/6$
S_{Ba}	S_{Bb}	S_{Ac}	+7	$2/3v_{AB}$	$4\pi/3$	$2/\sqrt{3}i_c$	$-\pi/6$
S_{Aa}	S_{Ab}	S_{Bc}	−7	$-2/3v_{AB}$	$4\pi/3$	$-2/\sqrt{3}i_c$	$-\pi/6$
S_{Ca}	S_{Cb}	S_{Bc}	+8	$2/3v_{BC}$	$4\pi/3$	$2/\sqrt{3}i_c$	$\pi/2$
S_{Ba}	S_{Bb}	S_{Cc}	−8	$-2/3v_{BC}$	$4\pi/3$	$-2/\sqrt{3}i_c$	$\pi/2$
S_{Aa}	S_{Ab}	S_{Cc}	+9	$2/3v_{CA}$	$4\pi/3$	$2/\sqrt{3}i_c$	$7\pi/6$
S_{Ca}	S_{Cb}	S_{Ac}	−9	$-2/3v_{CA}$	$4\pi/3$	$-2/\sqrt{3}i_c$	$7\pi/6$
S_{Aa}	S_{Ab}	S_{Ac}	0_1	0	—	—	0
S_{Ba}	S_{Bb}	S_{Bc}	0_2	0	—	—	0
S_{Ca}	S_{Cb}	S_{Cc}	0_3	0	—	—	0

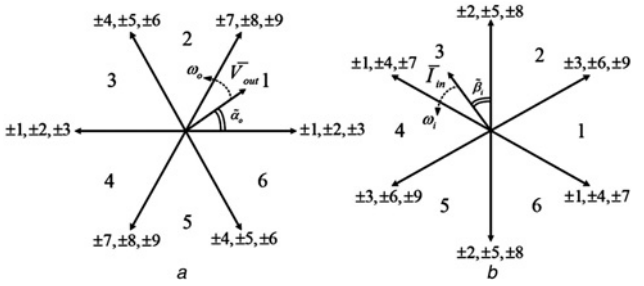

Fig. 2 *Active space vectors of*
a Output voltage
b Input current

configurations must be selected. Table 2 represents the active switching configurations for all possible combinations of the output voltage and input current vectors positions. To obtain the duty cycles of the active switching states, the reference vectors can be written as follows [15]

$$\bar{V}(1)d_3 + \bar{V}(2)d_4 = \bar{V}_{0a} = \frac{2}{\sqrt{3}} V_{\text{ref}} \sin(\tilde{\alpha}_o) e^{j[(K_v-1)(\pi/3)]} \quad (9)$$

$$\bar{V}(7)d_1 + \bar{V}(8)d_2 = \bar{V}_{0b} = \frac{2}{\sqrt{3}} V_{\text{ref}} \times \sin\left(\frac{\pi}{3} - \tilde{\alpha}_o\right) e^{j[(K_v-1)(\pi/3)+(\pi/3)]} \quad (10)$$

$$(\bar{I}(7)d_1 + \bar{I}(1)d_3).je^{j\tilde{\beta}_i+\pi/6} e^{j[(K_i-1)(\pi/3)]} = 0 \quad (11)$$

$$(\bar{I}(2)d_4 + \bar{I}(8)d_2).je^{j\tilde{\beta}_i+\pi/6} e^{j[(K_i-1)(\pi/3)]} = 0 \quad (12)$$

in which K_v and K_i are the number of sectors which the output voltage and the input current vectors located in, respectively, '.' donates the scalar product operator and

$$\tilde{\alpha}_o = \alpha_o - (K_v - 1)\frac{\pi}{3}, \quad \tilde{\beta}_i = \beta_i - (K_i - 1)\frac{\pi}{3} \quad (13)$$

where α_o and β_i are the phase angles of the output voltage and the input current vectors, respectively. Solving (9) to (12), the duty cycles are derived as

$$d_1 = (-1)^{K_v+K_i} \frac{2}{\sqrt{3}} q \frac{\sin(\tilde{\alpha}_o)\sin(\tilde{\beta}_i)}{\cos\varphi_i} \quad (14)$$

$$d_2 = (-1)^{K_v+K_i+1} \frac{2}{\sqrt{3}} q \frac{\sin(\tilde{\alpha}_o)\sin((\pi/3)-\tilde{\beta}_i)}{\cos\varphi_i} \quad (15)$$

$$d_3 = (-1)^{K_v+K_i+1} \frac{2}{\sqrt{3}} q \frac{\sin((\pi/3)-\tilde{\alpha}_o)\sin(\tilde{\beta}_i)}{\cos\varphi_i} \quad (16)$$

$$d_4 = (-1)^{K_v+K_i} \frac{2}{\sqrt{3}} q \frac{\sin((\pi/3)-\tilde{\alpha}_o)\sin((\pi/3)-\tilde{\beta}_i)}{\cos\varphi_i} \quad (17)$$

where q is the VTR defined as the ratio of the output voltage amplitude to the input voltage amplitude.

Considering (14)–(17), it is obvious that two of these duty cycles are always negative. In the case of negative duty cycles, the corresponding negative switching configurations should be chosen rather than the positive ones from Table 2.

To complete the switching cycle, zero configurations are added as

$$\sum_{i=1}^{4} |d_i| + \sum_{j=1}^{3} d_{0_j} = 1 \quad (18)$$

In (18), d_{0j} indicates the duty cycle of jth zero vector in Table 1.

3 SVM capacity to achieve higher VTRs

To examine the maximum instantaneous VTR of SVM, zero duty cycles are considered null, that is

$$\sum_{i=1}^{4} |d_i| = 1 \quad (19)$$

Substituting (14) to (17) in (19), the maximum achievable

Table 2 Used switching states for each combination of output voltage and input current vectors position

		Sector of output voltage vector											
		1 or 4				2 or 5				3 or 6			
Sector of input current vector	1 or 4	±9	±7	±3	±1	±6	±4	±9	±7	±3	±1	±6	±4
	2 or 5	±8	±9	±2	±3	±5	±6	±8	±9	±2	±3	±5	±6
	3 or 6	±7	±8	±1	±2	±4	±5	±7	±8	±1	±2	±4	±5
		d_1	d_2	d_3	d_4	d_1	d_2	d_3	d_4	d_1	d_2	d_3	d_4

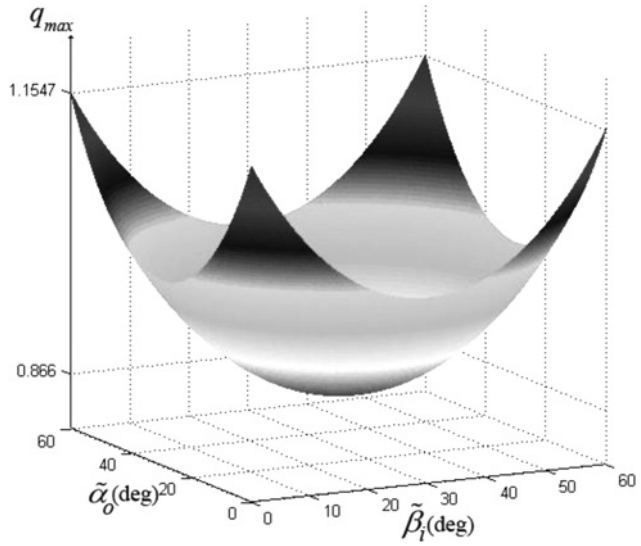

Fig. 3 *Instantaneous maximum VTR as a function of* $\tilde{\alpha}_o$ *and* $\tilde{\beta}_i$

VTR is attained as

$$q_{\max} = \frac{\sqrt{3}}{2} \frac{|\cos \varphi_i|}{\sin(\tilde{\alpha}_o + (\pi/3)) \sin(\tilde{\beta}_i + (\pi/3))} \tag{20}$$

As the equation reveals, the maximum VTR depends on the position of the output voltage and the input current vectors. Assuming $|\cos\varphi_i| = 1$, variations of the maximum VTR as a function of $\tilde{\alpha}_o$ and $\tilde{\beta}_i$ can be represented as Fig. 3 (the variations of $\tilde{\alpha}_o$ and $\tilde{\beta}_i$ are within a sector, that is, [0°, 60°]). As the figure demonstrates, the minimum of the maximum instantaneous VTR is 0.866, known as the intrinsic limitation of the SVM. This condition occurs when both output voltage and input current vectors are located in the middle of their sectors (i.e. $\tilde{\alpha}_o = 30^\circ$ and $\tilde{\beta}_i = 30^\circ$). When both vectors are at the begininng or at the end of their sectors (i.e. $\tilde{\alpha}_o = 0^\circ$ or $\tilde{\alpha}_o = 60^\circ$, and $\tilde{\beta}_i = 0^\circ$ or $\tilde{\beta}_i = 60^\circ$), the maximum achievable VTR (1.15) will be attained.

4 Proposed space vector overmodulation for matrix converter

4.1 Similarities between VSI and matrix converter space vector overmodulation

Some successful attempts have been made in order to achieve higher modulation indices in SVM for VSIs [16, 17]. In [17], depending on the magnitude of the modulation index, two modes are adopted. When the modulation index is between 0.906 and 0.952, the first mode is selected. In mode I, while the reference voltage vector is inside the hexagonal region created by the active voltage vectors, the modulation is similar to the conventional SVM. Now, if the reference vector exceeds the hexagon boundaries, the duty cycles are chosen so that the tip of the reference vector lies on the sides of the hexagon (maximum VTR with no zero state). If the reference vector moves on the hexagon boundaries thoroughly, the upper limit of mode I is reached (MI = 0.952). For the modulation indices from 0.952 to 1, mode II is employed. In this mode, the reference vector moves along the sides of hexagon, and when it is placed at a certain distance from a hexagon vertex, it is held at the vertex for a particular time.

Despite basic similarities between the SVM for matrix converters and SVM for VSIs, there are notable differences between the SVM overmodulation for them. First of all, in the matrix converter modulation, two reference quantities should be controlled at the same time (the output voltage vector and the input current angle). Furthermore, in contrast with the SVM for VSIs, a given shape as the trajectory of the maximum VTR cannot be defined. As shown by (20), the trajectory of maximum instantaneous VTR of the matrix converter depends on the instantaneous phase angles of the output voltage and the input current vectors. It is simple to show that the ratio of the output frequency to the input frequency specifies the shape of trajectory. Clarifying the issue, $\tilde{\alpha}_o$ and $\tilde{\beta}_i$ are written in terms of time

$$\tilde{\alpha}_o = \omega_o t - \alpha_0 - (K_v - 1)\frac{\pi}{3} \tag{21}$$

$$\tilde{\beta}_i = \omega_i t - \beta_0 - (K_i - 1)\frac{\pi}{3} \tag{22}$$

in which α_0 and β_0 are the initial phase angles of the output voltage and the input current vectors, respectively. Now, (20) can be rewritten as (23).

$$q_{\max}(t) = \frac{(\sqrt{3}/2)|\cos \varphi_i|}{\sin(\omega_o t - \alpha_0 - (K_v - 1)(\pi/3) + (\pi/3)) \times \sin(\omega_i t - \beta_0 - (K_i - 1)(\pi/3) + (\pi/3))} \tag{23}$$

It is obvious that at each time instant, t, and for a given input frequency, ω_i, the value of maximum instantaneous VTR, $q_{\max}(t)$, is not a constant value and varies for different output frequencies, ω_o. Fig. 4 illustrates the trajectory of the maximum instantaneous VTR for four different output frequencies, when the input frequency is 50 Hz and $|\cos \varphi_i| = 1$.

These dissimilarities between the SVM for matrix converters and VSIs cause some complications in extending the SVM to the overmodulation region for matrix converters. Following the idea of [17] for VSIs overmodulation, a method for increasing the VTR for matrix converters is proposed which is divided into two modes based on the desired VTR.

4.2 Overmodulation mode I

In mode I, besides increasing the VTR beyond 0.866, the quality of reference quantities is of main concern. Hence, depending on the magnitude of desired VTR, when the desired VTR is lower than the maximum instantaneous VTR, the modulation is as the conventional SVM; otherwise, the duty cycles of active vectors are scaled such that the sum of them is limited to unity. In fact, once the original reference trajectory passes outside the trajectory of the maximum instantaneous VTR (Fig. 4), the time average equation (18) gives a negative duration for the zero vectors. To tackle this problem, the magnitude of the reference voltage is modified in order to keep the space vector within the trajectory. In other words, it implies that

$$\sum_{i=1}^{4} d_i' = 1 \tag{24}$$

in which d_i' is the modified duty cycle of the ith active vector

doi: 10.1049/iet-pel.2013.0740

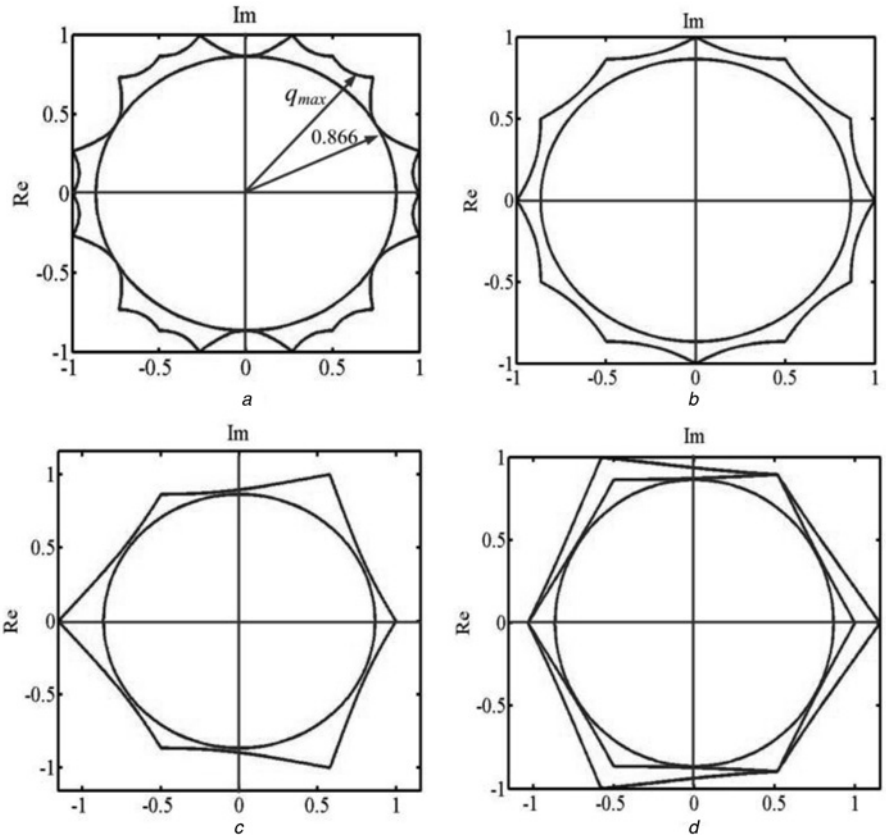

Fig. 4 *Trajectory of maximum instantaneous VTR for*
a $f_o = 25$ Hz
b $f_o = 50$ Hz
c $f_o = 100$ Hz
d $f_o = 200$ Hz and $f_i = 50$ Hz

in mode I, which is calculated as

$$d_i' = \frac{d_i}{d_1 + d_2 + d_3 + d_4}, \quad i = 1, \ldots, 4 \tag{25}$$

where d_i is obtained from (14) to (17). The output phase voltage waveforms for $m^* = 1.15$, without considering the switching effect (average mode), are depicted in Fig. 5 for $f_i = 50$ Hz and $f_o = 100$ Hz. Here, m^* denotes the magnitude of the desired VTR. It should be mentioned that for achieving the maximum VTR, the input power factor is considered unity for the entire analyses from now on. Fig. 6 represents the changes of the magnitude of the output phase voltage fundamental component, obtained from the Fourier transform, as a function of the output to input frequency ratio and m^*. As Fig. 6 reveals, in mode I, and for each output frequency, a certain maximum VTR is available. To reach higher ratios, another method must be employed.

4.3 Overmodulation mode II

As mentioned in Section 4.2, there is a maximum limit for the fundamental component of the output voltage in mode I, which the VTR cannot be improved further as shown in Fig. 6. Indeed, the maximum VTR is obtained when the reference vector always moves on the trajectory of the

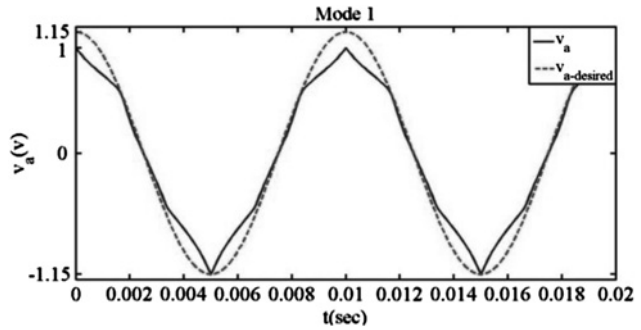

Fig. 5 *Output phase voltage waveform for $f_i = 50$ Hz, $f_o = 100$ Hz and $m^* = 1.15$ in mode I*

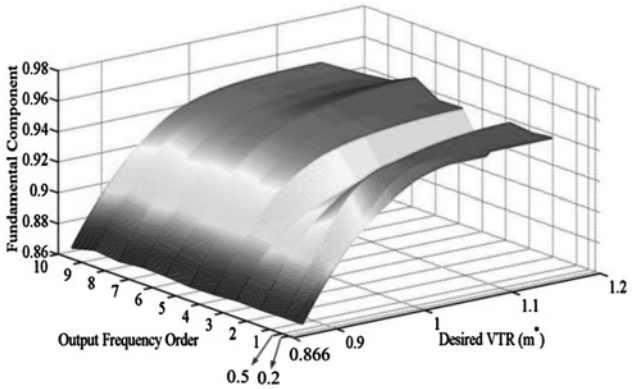

Fig. 6 *Magnitude of fundamental component as a function of output frequency order and desired VTR for $f_i = 50$ Hz in mode I*

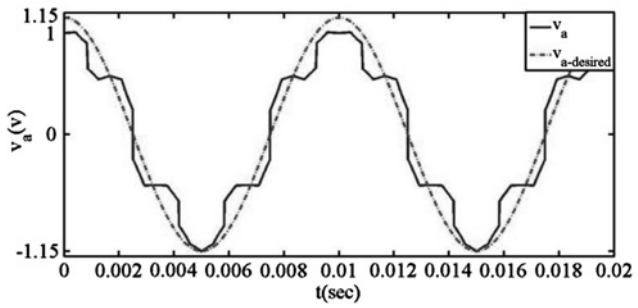

Fig. 7 *Output phase voltage waveform for $f_i = 50$ Hz, $f_o = 100$ Hz, $\zeta = \pi/12$ and $m^* = 1.15$ in mode II*

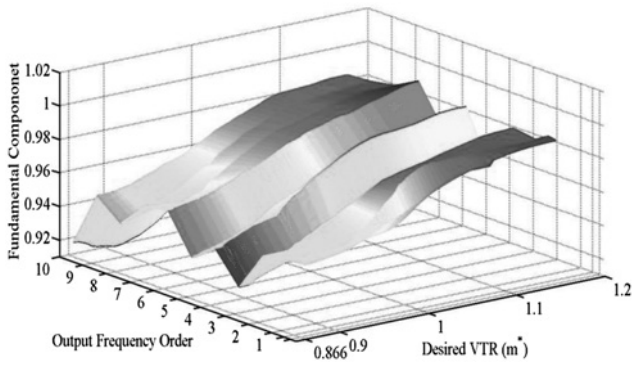

Fig. 8 *Magnitude of fundamental component as a function of output frequency order and desired VTR for $f_i = 50$ Hz and $\zeta = \pi/12$ in mode II*

maximum instantaneous VTR. In mode II, the output voltage vector is displaced to a position that according to (20) the higher instantaneous VTR can be yielded. Obviously, both amplitude and angle of the reference voltage vector are manipulated. As a consequence, the quality of the output voltage will decline. Considering the fact that the angle of the input current determines the input power factor, the input current vector position is maintained. Hence, the mode II will be as follows.

At the first stage, m^* and ζ are defined as the input variables; m^* is the desired VTR, and ζ indicates the search band around the output voltage vector angle to find the output voltage vector position with the desired VTR. Now, whenever m^* is lower than the maximum instantaneous VTR, the duty cycles are chosen as mode I, so that the output voltage vector can reach the maximum instantaneous VTR in that moment. In the case that m^* is higher than the maximum instantaneous VTR, the following equation is solved to find the position of the maximum VTR near the reference voltage vector, denoted by x

$$m^* - \frac{\sqrt{3}}{2}\frac{|\cos\varphi_i|}{\sin(x+(\pi/3))\sin(\tilde{\beta}_i+(\pi/3))} = 0 \qquad (26)$$

Owing to the sinusoidal nature of (26), there exist two answers. To reduce the distortion of the output voltage vector, the closer answer to the current position of the reference output voltage vector is chosen.

After obtaining the answer, two conditions should be checked. The first condition states that the new reference

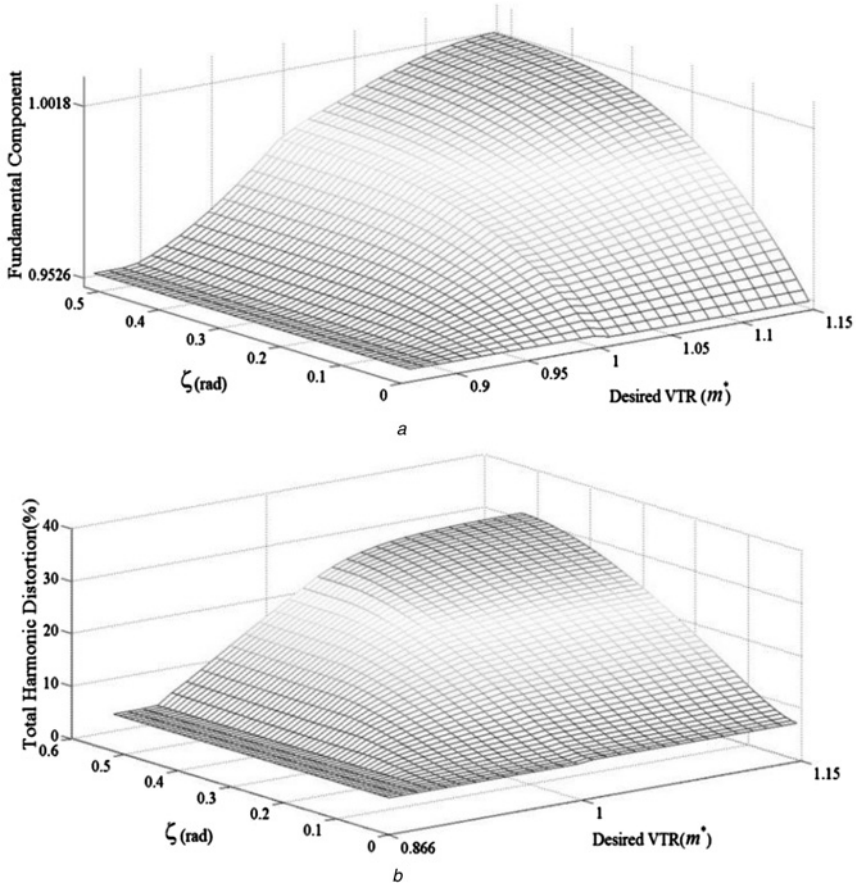

Fig. 9 *Maximum instantaneous fundamental component and the THD of the output voltage for $f_i = 50$ Hz in mode II*

a Maximum instantaneous fundamental component of output voltage in terms of ζ and desired VTR
b THD of output voltage in terms of ζ and desired VTR

doi: 10.1049/iet-pel.2013.0740

vector must not be out of the current sector of the reference output voltage vector

$$0 \le x \le \frac{\pi}{3} \tag{27}$$

If x is located inside the sector, it will be kept; otherwise, the closer sector bound to x is selected as the new answer. If x^* is the answer after the first condition, then it must meet the second condition. Second condition investigates whether the answer is inside the band defined by ζ. This condition can be expressed as

$$\tilde{\alpha}_o - \xi \le x^* \le \tilde{\alpha}_o + \xi \tag{28}$$

in which $\tilde{\alpha}_o$ is the current angle of the reference output voltage vector in the current sector. Now, if the answer satisfies (28), it will be the final answer; otherwise, the output voltage vector is transferred to the upper or lower bound of (28), whichever is closer to the current position of the reference output voltage vector.

Finally, if $\tilde{\alpha}_o^*$ is the new angle of the output voltage vector, the duty cycles will change as

$$d_i'' = \frac{d_1}{d_1 + d_2 + d_3 + d_4} \tag{29}$$

in which d_i are similar to (14) to (17), while $\tilde{\alpha}_o$ is replaced with $\tilde{\alpha}_o^*$. Fig. 7 shows the output voltage waveforms for $m^* = 1.15$, $\zeta = \pi/12$, $f_i = 50$ Hz and $f_o = 100$ Hz in mode II.

As Fig. 7 illustrates, in mode II, although the distortion of the output voltage in comparison with mode I is increased, the amplitude of the output voltage rises. The variation of the magnitude of the output phase voltage fundamental component in terms of output frequency and the desired

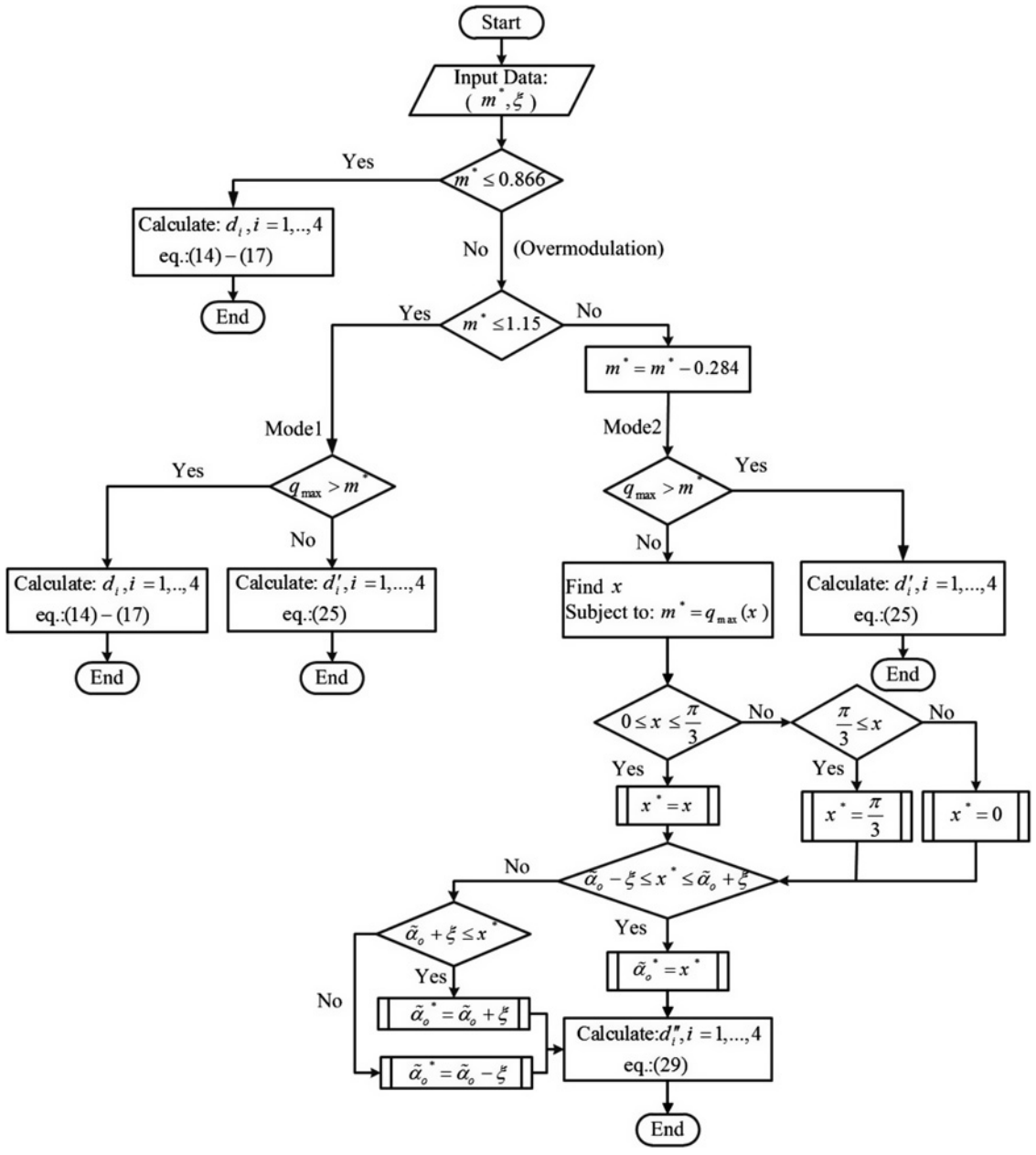

Fig. 10 *Flowchart of proposed space vector overmodulation method*

VTR in mode II and for $f_i = 50$ Hz and $\zeta = \pi/12$ is represented in Fig. 8.

Figs. 9*a* and *b* show the maximum instantaneous fundamental component of the output voltage and its THD as functions of ζ and m^*, respectively. As Fig. 9 demonstrates, increasing ζ leads to the rise of maximum instantaneous fundamental component of the output voltage and corresponding THD. The maximum VTR is obtained by the nearly six-step square-wave operation for $\zeta = \pi/6$ and $m^* = 1.15$.

As Fig. 9 reveals, the THD value is high in mode II and working in this mode is recommended only during the transients (e.g. a very fast speed change of a driven motor). Furthermore, as mentioned before, in matrix converter space vector overmodulation, there is no certain point as the transition boundary between two overmodulation modes for different output to input frequency ratios; therefore defining the switch point from modes I to II can be difficult. For having continuous operation, especially for closed-loop control, an algorithm depicted in Fig. 10 can be adopted. As the flowchart shows, if m^* is <0.866, duty cycles are calculated as the linear mode operation; otherwise, if m^* is <1.15, mode I is selected, and if m^* is >1.15, first 0.284 (1.15 − 0.866 = 0.284) is subtracted from m^*, then, the result is given as VTR input to mode II.

5 Performance evaluation

To testify the validity of the proposed method, some experiments have been conducted. The schematic circuit and the experimental test rig are shown in Figs. 11 and 12, respectively. The matrix converter parameters are summarised in Table 3. Owing to the safety issues, the input voltage decreased to 70 V. The matrix converter power circuit consists of 18 metal-oxide semiconductor field-effect transistor switches (IRFP460).

To implement the overmodulation method, a 32-bit floating-point digital signal controller (DSC) from Texas Instruments (TMS320F28335) operating at a clock frequency of 150 MHz is used. The measured input voltages are sampled at 10 kHz. The converter switching frequency is also decided to be 10 kHz. In each sampling period, after performing the overmodulation algorithm in the DSC, the switching states and the corresponding duty cycles are transferred to a field-programmable gate array (FPGA) board (Xilinx XC6SLX9 device from Spartan-6 family) through serial peripheral interface. The FPGA program uses this information to generate the gating signals for the power circuit. In addition, in order to achieve safe commutation between bidirectional switches, the four-step current-based switching method (FSSM) [18] is adopted. To perform FSSM, the output current sign is also fed to the FPGA. The drive circuit is composed of HCPL3120 gate driver integrated circuits and provides the gating pulses for the bidirectional switches.

In the first test, the conventional SVM algorithm for $m^* = 0.866$ is performed in condition that the THD of the grid voltage is 5.9%. As mentioned before, 0.866 is the maximum achievable VTR for the matrix converter under linear operation. Fig. 13*a* presents the input and output waveforms of the matrix converter. Sinusoidal current waveforms and the unity power factor at the input confirm that the reference quantities are synthesised properly. Also, by fast Fourier transform (FFT) analysis of the output phase voltage, the peak of fundamental component is calculated as 51.1 V; therefore VTR is obtained as 0.8517 (VTR = 51.1/60) instead of 0.866. The small deviation from the reference can be attributed to the voltage drop on the input filter and the semiconductor switches. In this condition, the

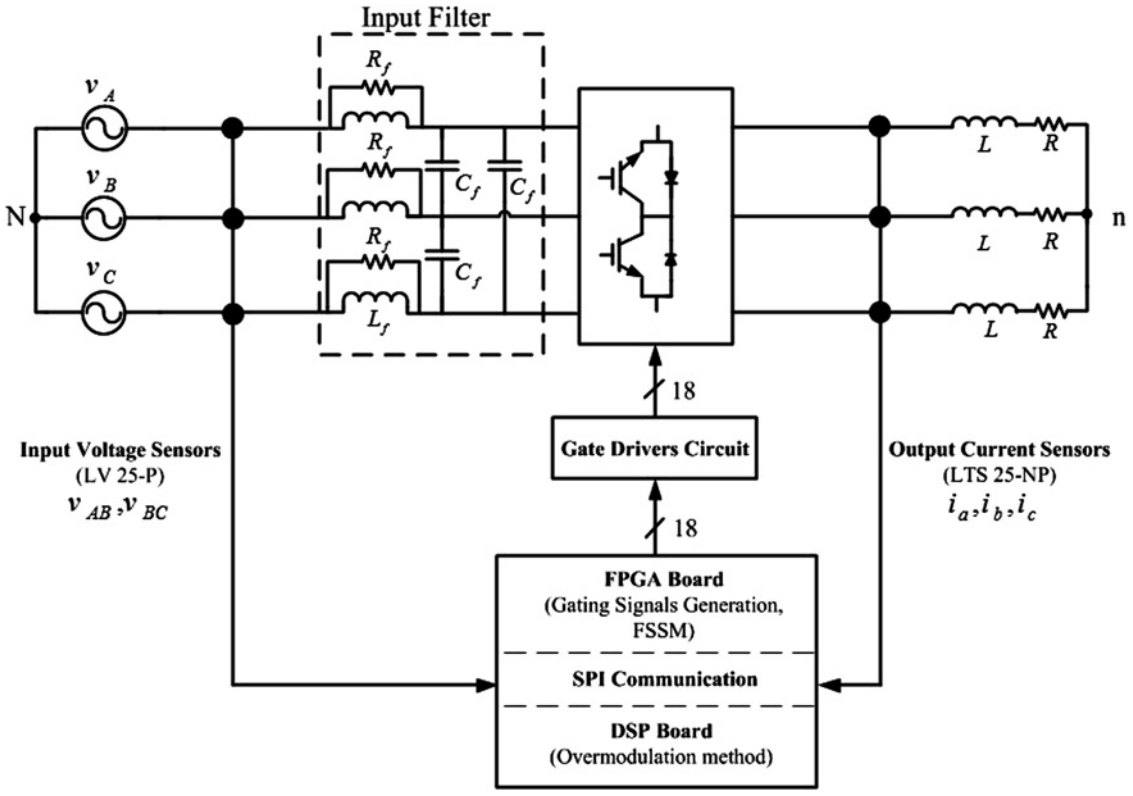

Fig. 11 *Block diagram of experimental test rig*

doi: 10.1049/iet-pel.2013.0740

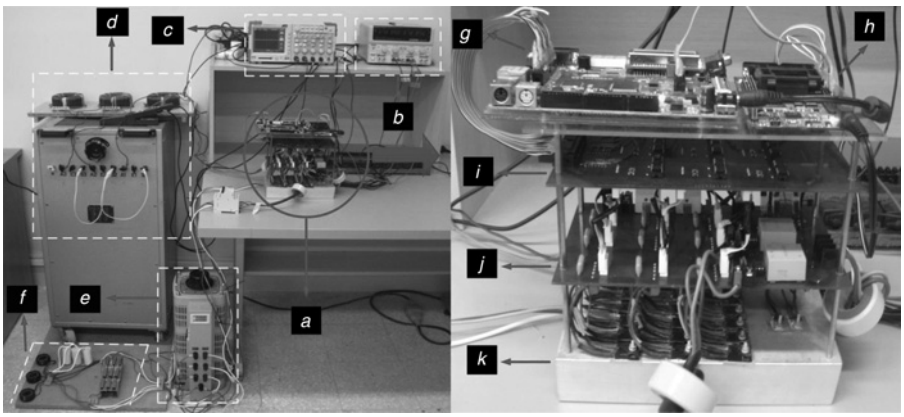

Fig. 12 *Matrix converter experimental test rig*

a Matrix converter circuit
b Supply
c Oscilloscope
d *R–L* load
e Input transformer
f Input filter
g FPGA board
h DSC board (eZdspF28335)
i Gate drive circuit
j Measurements circuit
k Bidirectional switches on the heat sink

Table 3 Matrix converter parameters

R–L load	$R = 6\ \Omega$, $L = 10$ mH
input filter	$R_f = 10\ \Omega$, $L_f = 1$ mH, $C_f = 8\ \mu$F
switching frequency	10 kHz
f_i	50 Hz
f_o	100 Hz
input voltage(line-to-line rms)	70 V
power factor	1

input and output current THDs are 6.7 and 3.66%, respectively.

The output voltage and current waveforms for $m^* = 1.15$ in overmodulation mode I are depicted in Fig. 13*b*. The FFT analysis shows that the peak value of the output phase voltage reaches 55.76 V (VTR = 0.929), whereas the output current THD is 5.29%. In addition, as the figure depicts, the

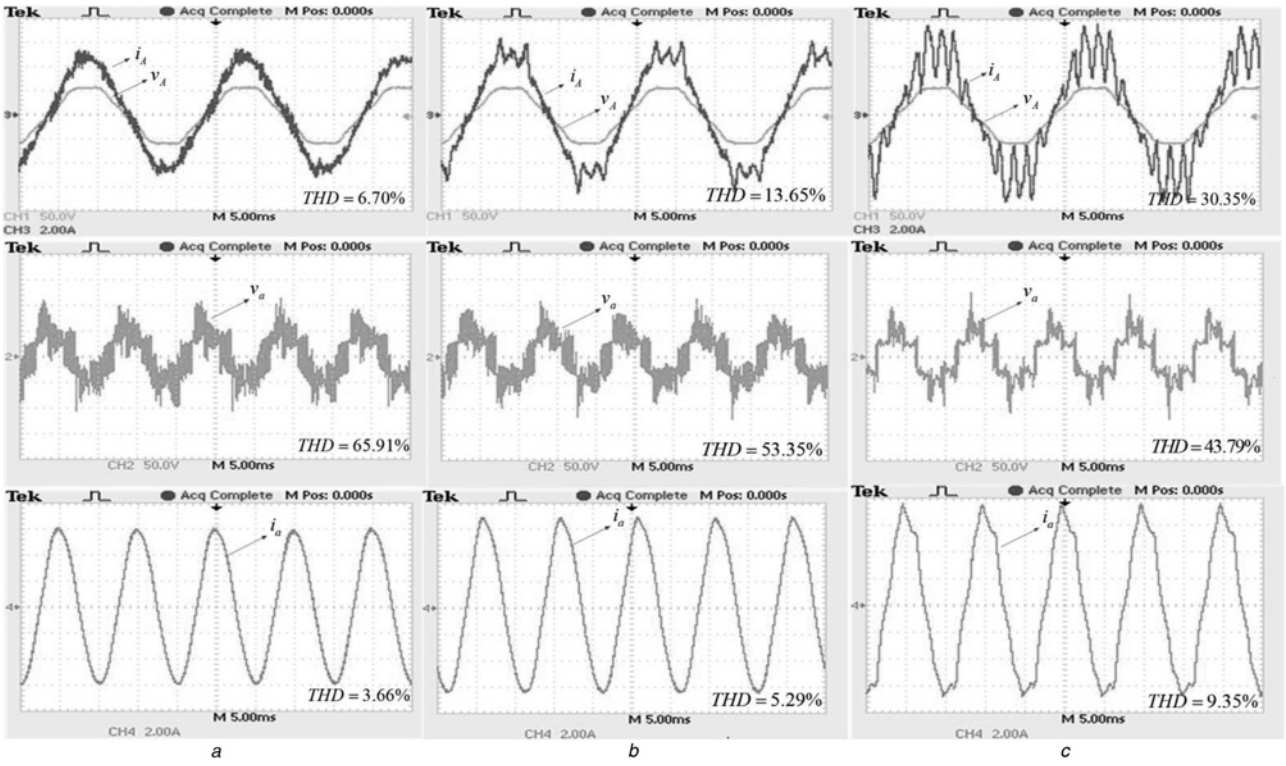

Fig. 13 *Experimental waveforms for*

a Linear modulation and $m^* = 0.866$
b Overmodulation mode I and $m^* = 1.15$
c Overmodulation mode II, $\zeta = \pi/12$ and $m^* = 1.15$

THD of the input current has raised to 13.65% which shows a large increase compared with the linear modulation mode.

In the final test, mode II has been executed, and $m^* = 1.15$ and $\zeta = \pi/12$ are chosen as the input parameters. The experimental waveforms are shown in Fig. 13*c*. The voltage produced by the converter is a quasi-six-step waveform and the switching frequency is highly reduced, as expected. The VTR reaches 0.985 in this case (VTR = 59.1/60), which means an increase of 7% compared with its value in mode I. However, the THD of the input and output currents increases from 5.29 and 13.65% (in mode *I*) to 9.35 and 30.35% in mode II, respectively. Considering the input current waveforms of Figs. 13*a–c* reveals that while the displacement remains almost zero, the amplitude of low-order harmonics dramatically increases for overmodulation operation. Obviously, the control of input current is sacrificed to extend the VTR of the matrix converter in overmodulation methods, especially in mode II. Consequently, this method should be used just during transient operations. Also, in the case of frequent transitions to overmodulation modes, special care must be taken in the design of input filter to prevent the high-amplitude harmonic currents from flowing into the supply side.

6 Conclusion

In this paper, the existence capacity of SVM to reach higher VTRs has been examined. A new overmodulation method including two modes has been presented. Through experimental tests, the feasibility of the proposed method is demonstrated. Extending the VTR up to unity, simplicity of implementation and rather small THD in the output quantities are the main characteristics associated to the presented overmodulation method. High distortion in the input current emphasises the need for redesigning the input filter when the overmodulation operation is used frequently.

7 References

1 Rodriguez, J., Rivera, M., Kolar, J.W., Wheeler, P.W.: 'A review of control and modulation methods for matrix converters', *IEEE Trans. Ind. Electron.*, 2012, **59**, (1), pp. 58–70

2 Empringham, L., Kolar, J.W., Rodriguez, J., Wheeler, P.W., Clare, J.C.: 'Technological issues and industrial application of matrix converters: a review', *IEEE Trans. Ind. Electron.*, 2013, **60**, pp. 4260–4271

3 Geyer, T., Papafotiou, G., Morari, M.: 'Model predictive direct torque control – Part I: concept, algorithm, and analysis', *IEEE Trans. Ind. Electron.*, 2009, **56**, (6), pp. 1894–1905

4 Klumpner, C., Blaabjerg, F., Boldea, I., Nielsen, P.: 'New modulation method for matrix converters', *IEEE Trans. Ind. Electron.*, 2006, **42**, (3), pp. 797–806

5 Alesina, A., Venturini, M.: 'Solid-state power conversion: a Fourier analysis approach to generalized transformer synthesis', *IEEE Trans. Circuits Syst.*, 1981, **28**, pp. 319–330

6 Alesina, A., Venturini, M.: 'Analysis and design of optimum-amplitude nine-switch direct AC–AC converters', *IEEE Trans. Power Electron.*, 1989, **4**, pp. 101–112

7 Huber, L., Borojevic, D.: 'Space vector modulated three-phase to three-phase matrix converter with input power factor correction', *IEEE Trans. Ind. Appl.*, 1995, **31**, (6), pp. 1234–1246

8 Dabour, S.M., Rashad, E.M.: 'Analysis and implementation of space-vector-modulated three-phase matrix converter', *IET Power Electron.*, 2012, **5**, (8), pp. 1374–1378

9 Chiang, T.G., Itoh, J.: 'Comparison of two overmodulation strategies in an indirect matrix converter', *IEEE Trans. Ind. Electron.*, 2013, **60**, (1), pp. 43–53

10 Fedyczak, Z., Szczesniak, P., Korotyeyev, I.: 'Generation of matrix-reactance frequency converters based on unipolar PWM AC matrix-reactance choppers'. Specialists Conf. in Power Electronics, June 2008, pp. 1821–1827

11 Satish, T., Mohapatra, K.K., Mohan, N.: 'Steady sate over-modulation of matrix converter using simplified carrier based control'. 33rd Annual Conf. Industrial Electronics Society, Taipei, November 2007, pp. 1817–1822

12 Ziogas, P.D., Khan, S.I., Rashid, M.H.: 'Analysis and design of forced commutated cycloconverter structures with improved transfer characteristics', *IEEE Trans. Ind. Electron.*, 1986, **33**, pp. 271–280

13 Yoon, Y.-D., Sul, S.-K.: 'Carrier-based modulation technique for matrix converter', *IEEE Trans. Power Electron.*, 2006, **21**, (6), pp. 1691–1703

14 Kyo-Beum, L., Blaabjerg, F.: 'An improved DTC-SVM method for sensorless matrix converter drives using an overmodulation strategy and a simple nonlinearity compensation', *IEEE Trans. Ind. Electron.*, 2007, **54**, (6), pp. 3155–3166

15 Casadei, D., Serra, G., Tani, A., Zarri, L.: 'Matrix converter modulation strategies: a new general approach based on space-vector representation of the switch state', *IEEE Trans. Ind. Electron.*, 2002, **49**, (2), pp. 370–381

16 Kerkman, R.J., Leggate, D., Seibel, B.J., Rowan, T.M.: 'Operation of PWM voltage source-inverters in the overmodulation region', *IEEE Trans. Ind. Electron.*, 1996, **43**, (1), pp. 132–141

17 Lee, D.-C., Lee, G.-M.: 'A novel overmodulation technique for space-vector PWM inverters', *IEEE Trans. Power Electron.*, 1998, **13**, pp. 1144–1151

18 Burany, N.: 'Safe control of four-quadrant switches'. Proc. Conf. IEEE Industry Applications Society Annual Meeting, San Diego, CA, 1989, pp. 1190–1194

doi: 10.1049/iet-pel.2013.0740